Turing Patterns, Spatial Bistability, and Front Instabilities in a Reaction−Diffusion System

István Szalai[†] and Patrick De Kepper*

Centre de Recherche Paul Pascal, CNRS Bordeaux, Avennue Schweitzer, F-33600 Pessac, France

Received: February 24, 2004; In Final Form: April 6, 2004

The chlorine dioxide−iodine−malonic acid oscillating reaction produces Turing patterns when operated in open spatial reactors. In the same operating conditions, the chlorine dioxide−iodide bistable reaction leads to spatial bistability between two steady states that do not break the symmetry of boundary conditions. We develop a system combining these two properties. Phase diagram studies show that the Turing pattern region cannot be generically made to interact with the phenomenon of spatial bistability. In the spatial bistability region, stationary pulses and complex transient domain patterns are observed, a new phenomenon for the chlorite−iodide driven systems. These have no connection with the previously observed Turing patterns. We propose a systematic design method to produce permanent domain patterns in systems exhibiting spatial bistability.

Introduction

The study of chemical reaction−diffusion patterns has become a stimulating and productive field of nonlinear dynamics.[1−4] The existence of stationary spatial patterns in reaction−diffusion systems was predicted more than fifty years ago by Alan Turing.[5] Such stationary concentration patterns are found in systems containing competing activatory and inhibitory chemical mechanisms with species exhibiting differences in diffusion coefficients. Two variable kinetic models give rise to Turing patterns only if the effective diffusion coefficient of the activator is sufficiently less than that of the inhibitory species—i.e., "short-range activation".[6] The chlorine dioxide−iodine−malonic acid (CDIMA) reaction[7] is the most dependable and widely used chemical system for the study of Turing patterns.[8−10] In this system many aspects of patterns were studied: one-, two-[8] and three-dimensional[10] asymptotic stationary patterns, interaction between the Turing instability and the oscillatory Hopf instability,[11] pattern growth dynamics,[12] and the effect of temporary or permanent spatiotemporal forcing on the pattern mode selection and on the wavelength.[13]

All these experiments were performed in open spatial reactors consisting of a piece of gel in contact with the contents of a continuous stirred tank reactor (CSTR).[14] The reactants and products are continuously exchanged between the gel part and the CSTR. The gel medium avoids convective transport and thus enables chemical patterns resulting from the sole interplay between reaction and diffusion to develop. One of the most popular spatial reactor configurations is that of the one-side fed reactor (OSFR) made of a thin disk of gel.[8,13] They are often assumed to approximate a uniformly constrained two-dimensional system, a geometry that is commonly used in model simulations. Recently, a phenomenon, named "spatial bistability", was found in this type of reactor and was studied both experimentally[15] and theoretically,[16] in connection with reaction systems that lead to temporal bistability when operated in a standard CSTR. This spatial bistability phenomenon corresponds to overlapping domains of stability of two different states in the gel for the same state of the CSTR. These states preserve the symmetry imposed by the feed at the boundary. One of the main lessons of these studies is that besides the feed composition, the thickness of the system can be a major parameter for the dynamics of systems operated in an OSFR. To study this phenomenon, annular-shaped OSFRs were designed to follow and clearly differentiate the different reaction states that develop in the depth of the gel. The first experimental demonstration was done with the chlorine dioxide−iodide (CDI) reaction.[15] Later, spatial bistability was also found in the pH-driven autocatalytic chlorite−tetrathionite reaction.[17] Spatial bistability should be a common phenomenon when self-activated reactions are operated in an OSFR. In extended systems exhibiting spatial bistability, one can generate an interface (front) between the two spatial states by making an appropriate local perturbation. The direction of propagation of such an interface depends on the relative stability of the stationary states and this direction can be reverted by changing the value of a control parameter.[15]

A large variety of spatial patterns[18] arising from transverse front instabilities and domain front interaction were found in the ferrocyanide−iodate−sulfite (FIS)[19] system. Labyrinthine patterns, self-replicating and oscillating spots, and wave repulsion were observed in this reaction when operated in a disk-shaped OSFR. The experiments were essentially carried on in regions of parameters where the reaction exhibits temporal bistability in a standard CSTR. The authors show[18] the existence of two distinct uniform steady states in the plane of the disk of gel. Contrary to the Turing patterns in the CDIMA reaction that develop spontaneously from a uniform state, beyond a critical parameter value, appropriate temporary or locally permanent (i.e., gel reactor defects) perturbations were necessary to initiate the front patterns. The theoretical studies[20] show that differences between the diffusion coefficients of the activator and the inhibitor species, analogous to those necessary for Turing patterns, play a central role in the pattern formation mechanism in the FIS reaction, though the actual origin of these diffusivity differences have not been determined, yet.

Here, we use a combination of the CDIMA[8] and CDI[15] reactions to investigate possible interactions between the Turing instability and the spatial bistability phenomenon and seek for different classes of domain patterns.

* Author to whom correspondence should be addressed. E-mail address: dekepper@crpp.u-bordeaux.fr.

[†] Permanent address: Department of Inorganic and Analytical Chemistry, L. Eötvös University, P.O. Box 32, H-1518 Budapest 112, Hungary.

10.1021/jp049168n CCC: $27.50
Published on Web 05/28/2004

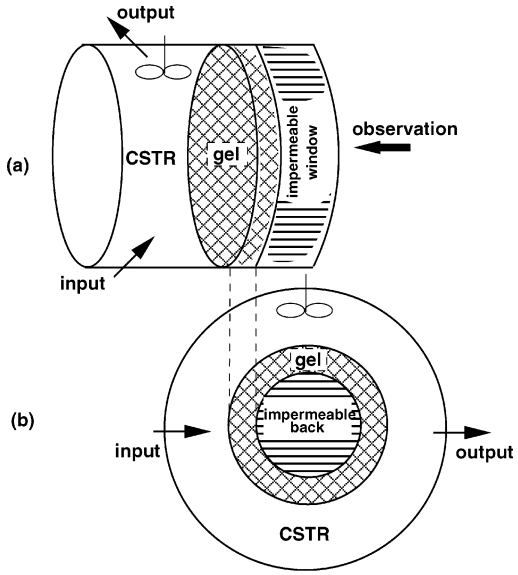

Figure 1. Sketches of the disk-shaped (a) and the annular one-side-fed reactors (b).

Experimental Conditions

A disk-shaped and an annular OSFR are sketched in Figure 1. Our disk-shaped OSFR consists of a thin disk of gel (diameter 18 mm, depth 1 mm), one face of which is in contact with the contents of a CSTR (volume 14 cm^3). The opposite face of the disk of gel is pressed against an impermeable window. A detailed description of such a reactor is given in ref 8. In this reactor, the observer only obtains an integrated value of light absorption across the thickness of the disk. To get a clear picture of the concentration distribution across the depth of the gel, a flat annular OSFR was used where all the sides of the annular gel (hight 0.2 mm, depth 1 mm), except the outer rim, are pressed against impermeable boundaries. The outer rim is in contact with the contents of a CSTR (volume 25 cm^3). A complete description is given in ref 15.

We used 2% agarose (Fluka 05070) gels in both cases. In all cases, the CSTR is continuously refreshed by constant flows of solutions of the initial reagents distributed in three separated reservoirs. The solutions are prepared with high-quality deionized water (Milli-Q, Millipore) and each contains 0.01 sulfuric acid. One reservoir contains a saturated solution of iodine (I_2) (Suptapur), at room temperature. A second reservoir contains a solution of chlorine dioxide (ClO_2) and PVA (Aldrich, 80% hydrolyzed, MW = 9000−10000) at 0 °C. PVA acts as a color indicator and reduces[22,23] the effective diffusion coefficient of the iodide ion (I^-), the activator. Both effects are connected to the formation a reversible reddish-purple PVA−I_3^- complex. ClO_2 is produced by acidic oxidation of sodium chlorite by sodium persulfate. The gaseous product is extracted from the liquor by air bubbling and redissolved in an ice-cold solution of 1 mol/dm^3 sulfuric acid.[24] The ClO_2 solutions are titrated by a standard iodometric volumetric method. The third reservoir contains variable amounts of potassium iodide (Prolabo) and malonic acid (MA) (Fluka). Equal flows are pumped (P500 pumps from Pharmacia) from the reservoirs and premixed just before being injected into the CSTR. The residence of the reactors is $\tau = 8$ min and they are thermostated at $T = 5$ °C. $[X]_0$ denotes the concentration, in units of mol/cm^3, that species X would have after mixing in the total inlet flow and prior to any reaction. During these experiments the $[I_2]_0$, $[ClO_2]_0$, and $[PVA]_0$ were fixed to 3.3×10^{-4}, 2×10^{-4}, and 10 g/dm^3 respectively. The qualitative changes of state of the CSTR contents were followed with a Pt electrode, the measured potential being mainly connected to the I^-/I_2 redox couple. The color intensity patterns were monitored by a CCD camera connected to a time lapse video recorder.

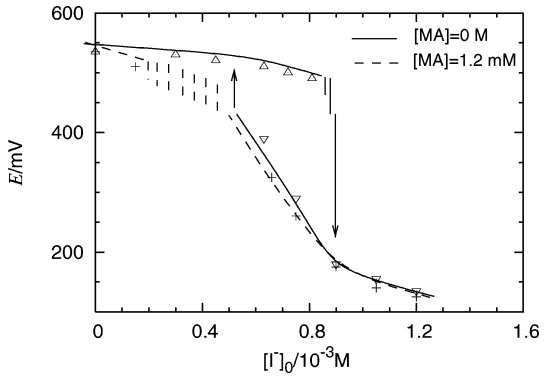

Figure 2. Dynamics of the CSTR. Potential E of an uncalibrated Pt electrode versus $Hg/Hg_2SO_4/K_2SO_4$ reference electrode. Stationary states: (△ and ▽) correspond, respectively, to the T and F branches in the absence of malonic acid, (+) in the presence of 1.2×10^{-3} of malonic acid. The vertical segments correspond to the amplitude of oscillatory states.

Experimental Results

Dynamics of the CSTR. Let us first describe the dynamics within the CSTR. Typical potential changes of the CSTR contents as a function $[I^-]_0$ are presented in Figure 2.

In the absence of malonic acid feed, the system is similar to the CDI reaction. It shows oscillations and bistability between two steady-state branches.[25] Like in the CDI reaction the introduction of PVA increases the range of bistability at the expense of the oscillatory domain.[15] However, our system differs by two aspects from the original CDI system: it is supplemented by an iodine feed and it is operated at a lower temperature. Starting from $[I^-]_0 = 0$ the CSTR remains on a high potential, low iodide concentration stationary state until $[I^-]_0 = 0.85 \times 10^{-3}$, where small amplitude oscillations appear. By convention we say that these low iodide states belong to the "thermodynamic" branch (T) because the composition of the CSTR is the continuation of the equilibrium state that one would obtain by decreasing the rate of the feed to zero. On further increasing $[I^-]_0$, the Pt potential drops; the contents of the CSTR switch to a low potential and high iodide concentration stationary state. Because this state is the continuation of that obtained in the high flow rate limit, we call it the "flow" state (F). When we decrease $[I^-]_0$, the F branch of states remains stable until $[I^-]_0 = 0.55 \times 10^{-3}$, where the contents of the CSTR switch back to the high potential steady state. In short, the system shows bistability between $[I^-]_0 = 0.55 \times 10^{-3}$ and $[I^-]_0 = 0.85 \times 10^{-3}$. Introducing MA reduces the range of the bistability and above $[MA]_0 = 0.7 \times 10^{-3}$ one can find only monostable steady and oscillatory states. The phase diagram of the CSTR (Figure 3) exhibits a standard cross-shaped topology.[26] We were not able to suppress these oscillations even by increasing the concentration of PVA up to 30 g/dm^3, but these oscillations have small amplitudes and do not lead to detectable oscillatory effects on the pattern formed in the gel.

In the absence of iodide feed, the system is identical to the CDIMA reaction. In this case by increasing $[MA]_0$, one can distinguish three states: a high potential steady state, an oscillatory state, and a lower potential steady state.[12] PVA has a quenching effect on the oscillatory dynamics and at $[PVA]_0 = 10$ g/dm^3, the value we used in our experiments, a smooth transition between the two steady states is obtained.[12]

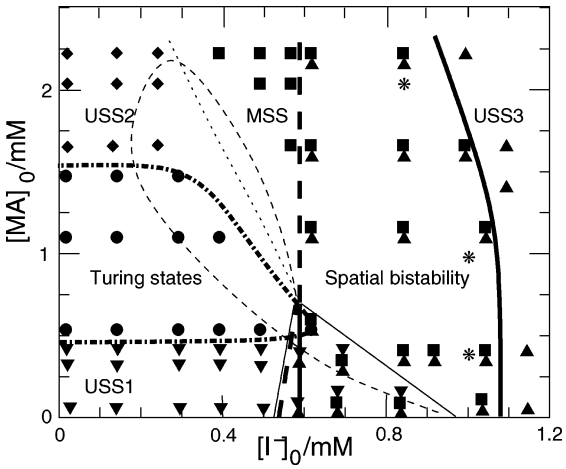

Figure 3. Experimental phase diagram in the ($[I^-]_0$, $[MA]_0$) plane. The symbols correspond the experimental points and are attributed to states of the gel: (▼) USS1; (▲) USS3; (■) MSS; (◆) USS2; (●) Turing state; (*) transient front patterns. Thin lines indicate the limits of the states in the CSTR: (—) limit of bistability; (---) limit of oscillations; (•••) limit between the high potential and the low potential branches. Thick lines indicate the limits of the states in the gel: (—) limit of the stability of the MSS; (---) limit of the stability of USS3; (-•-) limit of Turing states.

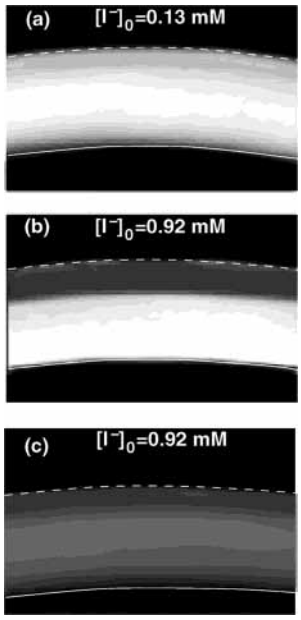

Figure 4. Asymptotic spatial states of the gel as a function of $[I^-]_0$ in the absence of malonic acid: (a) USS1 at $[I^-]_0 = 0.13 \times 10^{-3}$; (b) MSS and (c) USS3 states at $[I^-]_0 = 0.92 \times 10^{-3}$. The dotted curves indicate the CSTR/gel interface; the full curves delineate the location of the impermeable wall. Dark and clear regions inside the gel correspond, respectively, to high and low concentrations of the PVA−polyiodide colored complex.

Patterns in the Annular OSFR. Let us now describe the dynamics of the annular OSFR in the absence of MA. When the CSTR contents belong to the T branch, between $[I^-]_0 = 0$ and $[I^-]_0 = 0.85 \times 10^{-3}$, the gel is in a quasi-uniform pale-purple steady state (denoted USS1), which appears as a quasi-uniform pale-gray state in Figure 4a. At $[I^-]_0 = 0.85 \times 10^{-3}$, the CSTR contents start to oscillate but no visible qualitative change is observed in the gel annulus. On further increasing $[I^-]_0$, the CSTR contents switch to the F branch and simultaneously a new color distribution pattern settles in the annular gel (Figure 4b): a dark red-purple region develops along the outer rim whereas the inner part of the gel remains clear. The

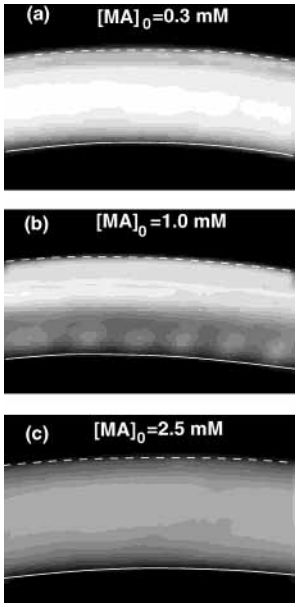

Figure 5. Asymptotic spatial states of the gel as a function of $[MA]_0$ in the absence of iodide: (a) USS1 at $[MA]_0 = 3 \times 10^{-4}$; (b) Turing state at $[MA]_0 = 1 \times 10^{-3}$; (c) USS2 at $[MA]_0 = 2.5 \times 10^{-3}$.

switch from the dark to the clear regions of the gel is very sharp and follows the symmetry imposed by the feed at the boundary. As mentioned above, the dark and clear regions indicate respectively regions of high and low iodide concentrations. We refer to such a mixed colored state as the mixed steady state (denoted MSS). Above $[I^-]_0 = 1.08 \times 10^{-3}$, the whole gel turns to a quasi-uniformly dark-purple state (denoted USS3). When $[I^-]_0$ is decreased, USS3 remains stable until the CSTR contents switch back to the T branch at $[I^-]_0 = 0.55 \times 10^{-3}$ (Figure 4c). Now, if we start again from the MSS and decrease $[I^-]_0$, the gel remains in this state until the CSTR contents jump to the T branch at $[I^-]_0 = 0.6 \times 10^{-3}$ and the gel switches to USS1. Between $[I^-]_0 = 0.6 \times 10^{-3}$ and $[I^-]_0 = 1.08 \times 10^{-3}$ two different spatial states, differing by their color profile across the depth of the gel, can be obtained for the same value of the feed and the same state of the CSTR: this is spatial bistability. At the intersection of the CSTR bistability and the spatial bistability of the gel the full system (CSTR + gel) is tristable (Figure 3).

In the absence of iodide in the feed, when the concentration of malonic acid is increased, one finds successively the USS1 (Figure 5a), a state exhibiting a stationary spot pattern for $0.5 \times 10^{-3} < [MA]_0 < 1.1 \times 10^{-3}$ (Figure 5b), and another quasi-uniform state (denoted USS2). The last state exhibits a distinct color from that of USS1. This corresponds to a medium gray level in Figure 5c. The spotted pattern (in the intermediate region) that appears spontaneously breaks the symmetry imposed by the feed at the boundary. These are Turing patterns. The preceding sequence of state is consistent with previous observations in the CDIMA reaction.[12]

In the full system, when both iodide and malonic acid are fed, the above description of states still holds except for the color profile of the mixed state. A new dark stripe emerges at the inner rim of the annulus, as MA is increased. Thus, the mixed state may exhibit a clear stripe (Figure 6) sandwiched between two darker regions. The dark inner stripe is due to the iodide recovery process associated with the reaction between MA and I_2. When $[I^-]_0$ increases, the clear stripe in the center of the annulus becomes thinner and thinner. At high $[I^-]_0$, at the limit of stability of the MSS, this stripe breaks into small

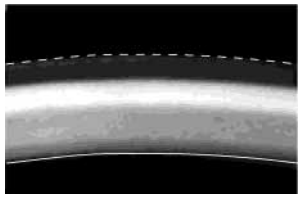

Figure 6. Asymptotic stable mixed state of the gel in the spatial bistability domain in the presence of malonic acid. Experimental conditions: $[MA]_0 = 2 \times 10^{-3}$, $[I^-]_0 = 0.92 \times 10^{-3}$.

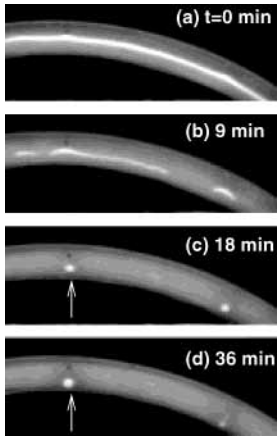

Figure 7. Transition from MSS to USS3 in the gel, stripe breaking, and transient spot growth in the annular reactor. Experimental conditions: $[I^-]_0 = 1.0 \times 10^{-3}$, $[MA]_0 = 7.0 \times 10^{-4}$.

segments that evolve into spots before disappearing completely (Figure 7). Once this critical $[I^-]_0$ value is reached, the stripe breaks within 10 min but the lifetime of the spots is between 0.5 and 1 h. In many cases the spots transiently grow in diameter. Then drift toward the impermeable wall and vanish (Figure 7d). These spots seem to have dynamics and a stability of their own.

One of the most remarkable features of the phase diagram in Figure 3 is that the range of the spatial bistability is significantly extended to higher $[MA]_0$ and shifted to higher $[I^-]_0$ compared with the range of the bistability of the CSTR. This differs from cases known previously where the range of parameter over which the spatial bistability develops is similar or smaller than the range of bistability of the CSTR itself. Note that, in a very small region of parameter, the Turing state and the spatial bistability are observed for the same values.

In the range of spatial bistability, a local perturbation with acidic chlorite can create interfaces (fronts) between the USS3 and the MSS. The direction of the propagation of the interface depends on the actual value of $[I^-]_0$, as was found already with the CDI reaction.[15] In the major fraction of the spatial bistability domain, the MSS propagates into the USS3. The turning point for the propagation direction is close to the high $[I^-]_0$ limit; e.g., at $[MA]_0 = 5.0 \times 10^{-4}$. This occurs approximately at $[I^-]_0 = 1.0 \times 10^{-3}$. Near this point, we could observe repulsion and stable front pairing phenomena between opposing interfaces (Figure 8d). In Figure 8, we can observe the evolution of four interfaces. In the first snapshot, two opposing interfaces are far from each other and two others are very close. The sequence of snapshots shows that the pairs of interfaces far apart move toward each other at ~0.8 mm/h and those that are in a close pair do not move. In the last snapshot, the distances between the two pairs of interfaces are similar and constant. This demonstrates that strong enough repulsions between colliding interfaces build up and enable the formation of stable pulses. Interestingly, the shape of interacting interfaces differs from that

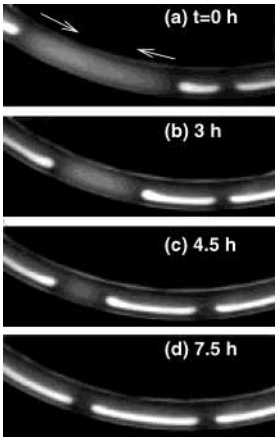

Figure 8. Formation of standing USS3 pulses in the MSS in the annular reactor. Snapshot (a) was taken 2 h after the initial perturbation. Experimental conditions: $[I^-]_0 = 1.0 \times 10^{-3}$, $[MA]_0 = 5.0 \times 10^{-4}$.

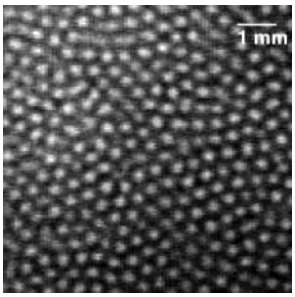

Figure 9. Typical Turing spot pattern observed in the disk reactor. Experimental conditions: $[I^-]_0 = 0.13 \times 10^{-3}$, $[MA]_0 = 1 \times 10^{-3}$.

of the moving ones. Depending on the experimental conditions, the stationary interface−pair distance ranges from 0.5 to 0.7 mm. Stable pulses of this type persist as long as control parameters remained unchanged. Their distribution along the ring is not periodic and depends on the initial conditions. These pulse widths are larger than the wavelength of the Turing patterns (~0.2−0.3 mm) observed in this system.

Patterns in the Disk-Shaped OSFR. The observed phase diagrams in the annular and the disk-shaped OSFR are identical within the experimental accuracy. In a disk-shaped OSFR, the Turing states are more easily observable than in the annular OSFR (Figure 9). The symmetry breaking patterns are better detected over the uniform background of the disk reactor than in the annular reactor where these patterns settle over in a color gradient. However, the determination of the spatial bistability limits is more difficult in a disk-shaped OSFR. The states are no more distinguished by a color profile but by a uniform value of transmitted light. This value is not unambiguous because the overall light absorption of the two states can be very similar. The phase diagram information established with the annular OSFR were systematically used to unambiguously test the limits of spatial bistability in the disk-shaped OSFR and to create interfaces between uniform regions of USS3 and MSS. The interface was initiated by indirect perturbations of the USS3, either by stopping the stirrer in the CSTR, or by making large temporary jumps in the $[I^-]_0$. In both cases, the fronts started from the edge of the disk.

We now describe different phenomena associated with the dynamics of this moving interface (front). When, after a sudden large jump in $[I^-]_0$, the MSS moves fast into the USS3, scattered clear spots transiently develop behind the interface. The spot pattern goes together with the formation of dark stripes laid down orthogonally to the interface. The stripe pattern is also

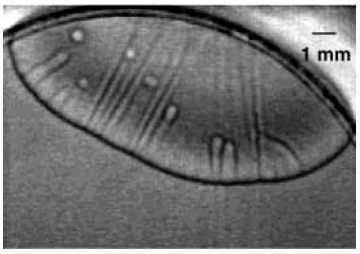

Figure 10. Transient pattern formation behind a propagating front after making perturbation by fast jumping from $[I^-]_0 = 0.9 \times 10^{-3}$ to $[I^-]_0 = 0.55 \times 10^{-3}$. Experimental conditions: $[MA]_0 = 1 \times 10^{-3}$.

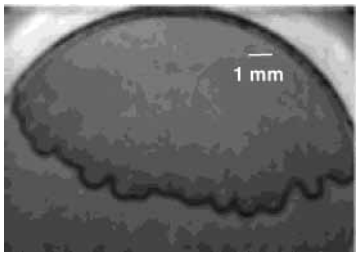

Figure 11. Illustration of transversal interface (front) instability in the disk reactor obtained after a local initial perturbation of the USS3. Experimental conditions: $[I^-]_0 = 0.73 \times 10^{-3}$, $[MA]_0 = 2.1 \times 10^{-3}$.

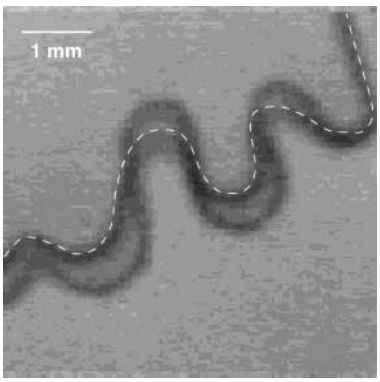

Figure 12. Curvature dependent interface (front) propagation in the disk reactor. The white dashed line indicates the original shape of the front, 10 min between the two snapshots. Experimental conditions: $[I^-]_0 = 0.77 \times 10^{-3}$, $[MA]_0 = 2.1 \times 10^{-3}$.

transient and seems to be triggered by a transversal front instability of short wavelength and amplitude (Figure 10). When the propagation of the interface is slower, the wavelength and the amplitude of this transversal instability increase, as illustrated in Figure 11. The dark part of the gel corresponds to the MSS and the lighter part corresponds to the USS3. By an appropriate change in the control parameter value, we could even observe changes in the direction of propagation, depending on the curvature sign of the interface. In Figure 12 the superposition of two snapshots taken at 10 min interval presents the evolution of an interface where the white dash line delineates the initial shape of the interface. In this situation, both the MSS and the USS3 are able to grow fingers into one another. If the repulsive interaction is strong enough to avoid the domain fusion, one can expect labyrinthine patterns to develop in this way.[21] In our experiments, we did not find conditions for which such patterns are asymptotically stable. However, a number of nontrivial dynamical patterns can temporarily develop during the transition from one uniform state domain to the other. The following scenarios can be observed. When, after a small change in control parameter value, fingers start to grow in opposite directions, as in Figure 12, the MSS also becomes globally unstable. Large patches of USS3 appear spontaneously inside the MSS regions. This corresponds to the local collapse of the clear middle stripe observed in the annular OSFR in similar conditions (Figure 7). In Figure 13, the first snapshot, taken several hours after the initial perturbation, shows islands of the USS3 in a gel that is mainly in the MSS (darker region). At this value of $[I^-]_0$, the USS3 propagates into the MSS, so that the islands of USS3 grow. In the region marked by an arrow in Figure 13b,c, the outburst of a new island is viewed. By following the evolution of this new patch, one can see that there is a strong repulsion between the limits of adjacent islands of USS3 and a strong dependence of the speed of the interface propagation on curvature. The patch that appears (Figure 13b) creates a new interface that propagates in the channel of MSS that was left between the two domains of USS3 (Figure 13c). The curved part at the top moves faster than the flatter parts. Head to head interfaces lock for a while at a critical distance. Remarkably, the flat interfaces at some time temporarily invert their direction of propagation so that from Figure 13b to Figure 13d, the stripes of the USS3 become thinner but, later, the spread of the USS3 overtakes again the MSS regions (Figure 13e,f). This surprising pulsation, which was repeatedly observed, is not understood. It could result from a global feedback of the gel composition on the CSTR contents, but test experiments with higher input flow rate in the CSTR did not qualitatively change observations. In snapshot Figure 13f, the relative distribution of states is inverted compared to the first snapshot: the MSS forms islands in the USS3. Ultimately, the whole disk fills uniformly with the USS3. In the region of parameters that we explored, we did not find sets of values for which such a domain pattern stabilizes, though they could persist for several hours. Small changes in $[I^-]_0$ by $\pm 5\%$ would readily make the MSS or USS3 become the asymptotically stable state. Increasing the concentration of PVA from 10 g/dm^3 (Figure 13) to 30 g/dm^3 (Figure 14) or decreasing the thickness of the gel from 1 to 0.3 mm had little effect on the stability of these patterns. The vertical orientation of the patterns in Figure 13 is most probably linked to a bias initiated by the flow stream that feeds the disk of gel. However, patterns that do not exhibit this effect, can also be observed as shown in Figure 14. The scenario shown in Figure 14 is the same as that in Figure 13. Large domains of the MSS (dark region) become unstable, and patches of the USS3 (clear regions) appear spontaneously. The repulsive interaction avoids the immediate fusion of these patches and leads to the formation of islands of mixed state. The labyrinthine-like pattern shown in Figure 14d is not stationary. All structures disappear after more than 2 h; the disk fills with the USS3. Many features of our patterns bear similarities with the labyrinthine pattern development[18] observed in the FIS reaction but ours are transient.

Discussion

We have examined pattern formation and front (interface) dynamics in an enriched chlorite−iodide driven system that can exhibit both Turing patterns and spatial bistability. One of the goals of this work was to determine if the Turing patterns and the phenomenon of spatial bistability, previously observed in separated subsystems, could be made to coexist for the same boundary conditions of the gel—i.e., for the same state of the CSTR. In this respect, the first conclusion is that the CSTR contents for Turing patterns and for spatial bistability belong to two different branches. The Turing patterns form when the contents of the CSTR belong to a direct extension of the thermodynamic branch whereas spatial bistability is restricted to a region where the CSTR contents belong to the flow branch.

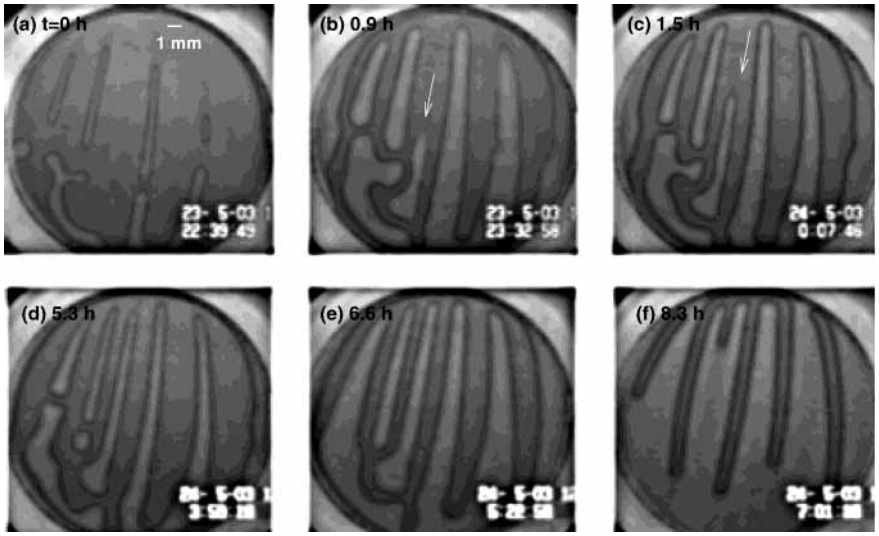

Figure 13. Dynamics of transient patterns obtained after initial perturbation of MSS in the disk reactor. Experimental conditions: $[I^-]_0 = 0.8 \times 10^{-3}$, $[MA]_0 = 2.1 \times 10^{-3}$, $[PVA]_0 = 10$ g/L.

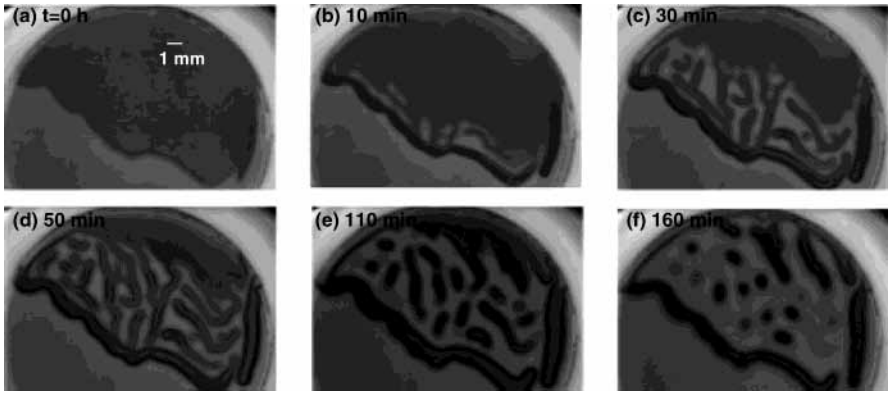

Figure 14. Transient pattern formation in the disk reactor. Experimental conditions: $[PVA]_0 = 30$ g/L, $[I^-]_0 = 1.0 \times 10^{-3}$, $[MA]_0 = 2.1 \times 10^{-3}$, $[PVA]_0 = 30$ g/L.

Turing patterns develop as an instability of the USS1 or USS2 states, never from the USS3 or MSS states. No interaction between the Turing patterns and the patterns issued from interacting fronts in the spatial bistability domain were found. However, this does not preclude that for other systems such a coexistence might be possible. In fact, recent model calculations in an extended Gray−Scott model show the development of Turing patterns on a mixed state.[27] Yet, even in this case, there is no straightforward relation between the above two classes of pattern forming processes. Nonetheless, there are numerical hints[28] that even in our particular chlorite−iodide driven system, but for other experimental conditions (chemical feed concentration, temperature, ...), another domain of spatial bistability, not associated to the branch of state found at high $[I^-]_0$, might exist and be able to overlap with the domain of Turing patterns.

Another feature of the phase diagram in Figure 3 is that the region of spatial bistability extends over a domain of feed parameters much larger than the domain of temporal bistability of the CSTR, contrary to observations in previous experiments. This experimental result and other observations from numerical simulations[28] of a detailed model of our enriched chlorite−iodide system suggest the fact that CSTR bistability is not a necessary requirement for the development of spatial bistability.

Our results clearly demonstrate that Turing patterns and standing patterns resulting from front interactions are not necessarily correlated phenomena in chemical systems. In our reaction system, they develop in very different domains of phase space, even if they rely on similar kinetic and diffusional prerequisites. We anticipate that this should be the standard case. The development of fronts requires the presence of an underlying pleated slow manifold (typical of systems exhibiting temporal bistability) in the system dynamics but this is unnecessary for Turing patterns. Thus, partial overlapping of the domains of the two types of standing spatial structures should not be generic.

This work contributes to the development of a systematic method to design in chemically different bistable or oscillatory reactions standing reaction−diffusion patterns resulting from front pairing interactions. The design method starts with finding spatial bistability in a one-sided continuously fed unstirred reactor. In the initial stage, it is strongly recommended to work in a spatial reactor that allows for the observation of concentration profiles within the depth of the gel reactor, like in the case of our annular OSFR. The first region to explore is naturally the one that corresponds to temporal bistability in the CSTR. As mentioned above, spatial bistability can extend widely beyond the CSTR bistability region but in the other regions one has no clear guideline for this quest. The second step in the method is to ensure conditions for the development of short-range activation. Though theoretically, this is not absolutely necessary condition in systems with more than two variables.[29] This space scale separation considerably helps, and the very large majority of theoretical model calculations made use of it. It is theoretically demonstrated that it is possible to reduce the

effective diffusivity of a small weight species by introducing immobile functional sites in the system that would reversibly bind this species.[22,23] Short-range activation can be provided if such a species controls the activatory kinetic path of the reaction. This is just what complexing agents such as starch or PVA do by binding polyiodide ions in the chlorite−iodide driven systems and polycarboxylate ions[30] do by binding protons in the pH-activated chlorite−tetrathionate reaction. The third step is to initiate interfaces between the two spatial states and explore the domains of parameters for which the direction of the propagation reverses. The final step is to study head-on collisions of interfaces in the neighborhood of the zero velocity region and search for conditions where nonvanishing front pairs would form.

Note that the dynamics of interfaces associated with steady state spatial bistability depends on the thickness of the gel reactors. This is naturally due to the development of concentration profiles of feed species across the gel. This is particularly dramatic for clock reactions where one of the feed species is directly involved in the patterning dynamics, as is the case for iodide ions in the CDI or in our present reaction system. In the CDI reaction, it was demonstrated, both theoretically and experimentally, that the thickness of the gel is a critical parameter both for the existence of spatial bistability and for the control of the direction of propagation of the interface.[15] In the case of the FIS reaction, patterns and pattern modes are also sensitively dependent on the gel thickness.[18]

In the case of stationary patterns, the feed by diffusion from the boundary must be able to counterbalance the overall consumption/production of dynamic species in the deepest part of the gel. A way to partly overcome this problem is to have an internal source of this species through slow reactions between major reactants that would remain in excess. Malonic acid and iodine just play such a role in the present system. This is probably why the increase in $[MA]_0$ helps to stabilize interface pairs. However, though stationary pulses were observed in the annular reactor, we were not able to produce stationary domain patterns in the disk reactor either by introducing malonic acid or by decreasing the thickness of the disk of gel. A dimensionality problem may also come into play to explain the stability difference between the patterns observed in the two different reactors. In the annular reactor, the interface only shows curvature in the direction perpendicular to the feed boundary whereas in the disk reactor patterns develop as "finger" in a plane parallel to the feed surface so that the interfaces between the USS3 and MSS states have an additional curvature. In fact, in the disk reactor, the transient patterns mostly vanish by retraction of the fingertips of one or the other domain states.

Though, in this work, we seem to be very close to conditions where stationary patterns originating in front interactions would form, the stability domain of these structures remained elusive. In consideration of the number of possible control parameters of the system, we have only explored a small part of the phase diagram. It would be tedious work to scan all the possible directions of phase space for such a system with six input chemical species plus temperature, CSTR residence time, and the thickness of the gel part. Clearly, the development of pattern in real open spatial reactors is an involved problem that requires practical guiding methods and further theoretical developments where boundary layer effects and feed parameter gradients would be explicitly considered.

Acknowledgment. This research has been supported by a Marie Curie Fellowship of the European Community program Improving Human Potential under contract number HPMF-CT-2002-011771. We thank J. Boissonade and D. Strier for helpful discussions.

References and Notes

(1) Field, R. J., Burger, M., Eds. *Oscillations and Traveling Waves in Chemical Systems*; Wiley: New York, 1985.
(2) Kapral, R., Showalter, K., Eds. *Chemical Patterns and Waves*; Kluwer Academic Publisher: Amsterdam, 1995.
(3) Epstein, I. R.; Pojman, J. *An Introduction to Nonlinear Chemical Dynamics*; Oxford University Press: New York, 1988.
(4) Borckmans, P.; Dewel, G.; De Wit, A.; Dulos, E.; Boissonade, J.; Gauffre, F.; De Kepper, P. *Int. J. Bif. Chaos* **2002**, *12*, 2307.
(5) Turing, A. M. *Philos. Trans. R. Soc. London, Ser. B* **1952**, *237*, 37.
(6) Murray, J. D. *Mathematical Biology I−II*; Springer-Verlag: Berlin, 2002.
(7) Lengyel, I.; Rábai, G.; Esptein, I. R. *J. Am. Chem. Soc.* **1990**, *112*, 4606.
(8) Rudovics, B.; Barillot, E.; Davies, P. W.; Dulos, E.; Boissonade, J.; De Kepper, P. *J. Phys. Chem. A* **1999**, *103*, 1790.
(9) Ouyang, Q.; Swinney, H. L. *Nature* **1991**, *352*, 610.
(10) Epstein, I. R.; Lengyel, I. *Physica D* **1995**, *84*, 1.
(11) Perraud, J. J.; De Wit, A.; Dulos, E.; De Kepper, P.; Dewel, G.; Borckmans, P. *Phys. Rev. Lett.* **1993**, *71*, 1272. De Kepper, P.; Perraud, J. J.; Rudovics, B.; Dulos, E. *Int. J. Bif. Chaos* **1994**, *4*, 1215.
(12) Davies, P. W.; Blanchedeau, P.; Dulos, E.; De Kepper, P. *J. Phys. Chem. A* **1998**, *102*, 8236.
(13) Ouyang, Q.; Gunaratne, G. H.; Swinney, H. L. *Chaos* **1993**, *3*, 707. Horváth, A. K.; Dolnik, M.; Munuzuri, A. P.; Zhabotinsky, A. M.; Epstein, I. R. *Phys. Rev. Lett.* **1999**, *83*, 2950. Berenstein, I.; Dolnik, M.; Zhabotinsky, A. M.; Epstein, I. R. *J. Phys. Chem. A* **2003**, *107*, 4428. Berenstein, I.; Lingfa, Y.; Dolnik, M.; Zhabotinsky, A. M.; Epstein, I. R. *Phys. Rev. Lett.* **2003**, *91*, 58302.
(14) Noszticzius, Z.; McCormick, W. D.; Swinney, H. L.; Tam, W. Y. *Nature* **1987**, *329*, 619.
(15) Blanchedeau, P.; Boissonade, J.; De Kepper, P. *Physica D* **2000**, *147*, 283.
(16) Blanchedeau, P.; Boissonade, J. *Phys. Rev. Lett.* **1998**, *81*, 5007.
(17) Boissonade, J.; Dulos, E.; Gauffre, F.; Kuperman, M. N.; De Kepper, P. *Faraday Discuss.* **2001**, *120*, 353. Fuentes, M.; Kuperman, M. N.; Boissonade, J.; Dulos, E.; Gauffre, F.; De Kepper, P. *Phys. Rew. E* **2002**, *66*, 56205.
(18) Lee, K. J.; McCormick, W. D.; Quyang, Q.; Swinney, H. L. *Science* **1993**, *261*, 192. Lee, K. J.; Swinney, H. L. *Phys. Rev. E* **1995**, *51*, 1899. Li, G.; Quyang, Q.; Swinney, H. L. *J. Chem. Phys.* **1996**, *105*, 10830.
(19) Edblom, E. C.; Orbán, M.; Epstein, I. R. *J. Am. Chem. Soc.* **1986**, *108*, 2826. Edblom, E. C.; Györgyi, L.; Orbán, M.; Epstein, I. R. *J. Am. Chem. Soc.* **1987**, *109*, 4876. Gáspár, V.; Showalter, K. *J. Am. Chem. Soc.* **1987**, *109*, 4869. Gáspár, V.; Showalter, K. *J. Phys. Chem.* **1990**, *94*, 4973.
(20) Pearson, J. E. Science, **1993**, *261*, 189. Muratov, C. B.; Osipov, V. V. *Phys. Rev. E* **1996**, *54*, 4860.
(21) Hagberg, A.; Meron, E. *Chaos* **1994**, *4*, 477.
(22) Lengyel, I.; Epstein, I. R. *Proc. Natl. Acad. Sci. U.S.A.* **1992**, *89*, 3977.
(23) Pearson, J. E.; Bruno, W. J. *Chaos* **1992**, *2*, 513.
(24) Nagypál, I. Private communication.
(25) Lengyel, I.; Li, J.; Esptein, I. R. *J. Phys. Chem.* **1992**, *96*, 7032.
(26) Boissonade, J.; De Kepper, P. J. *Phys. Chem.* **1980**, *84*, 501.
(27) Benyaich, K.; Métens, S.; Borckmans, P. Private communication.
(28) Strier, D. Private communication.
(29) Vastano, J. A.; Pearson, J. E.; Horsthemke, W.; Swinney, H. L. *Phys. Lett. A* **1987**, *124*, 320.
(30) Tóth, Á.; Lagzi, I.; Horváth, D. *J. Phys. Chem.* **1996**, *100*, 14837.